

# A DETECTION OF DARK MATTER HALO ELLIPTICITY USING GALAXY CLUSTER LENSING IN SDSS

ANNA KATHINKA DALLAND EVANS<sup>1</sup>, SARAH BRIDLE<sup>2</sup>

*Draft version October 24, 2018*

## ABSTRACT

We measure the ellipticity of isolated clusters of galaxies in the Sloan Digital Sky Survey (SDSS) using gravitational lensing. We stack the clusters, rotating so that the major axes of the ellipses determined by the positions of cluster member galaxies are aligned. We exclude the signal from the central  $0.5 h^{-1}$  Mpc to avoid problems with stacking alignment and cluster member contamination. We fit an elliptical NFW profile and find a projected, two-dimensional axis ratio for the dark matter of  $f = b/a = 0.48^{+0.14}_{-0.09}$  ( $1\sigma$ ), and rule out  $f = 1$  at 99.6 per cent confidence thus ruling out a spherical halo. We find that the ellipticity of the cluster galaxy distribution is consistent with being equal to the dark matter ellipticity. The results are similar if we change the isolation criterion by 50 per cent in either direction.

*Subject headings:* cosmology: dark matter — cosmology: galaxy clusters — cosmology: large-scale structure of universe — cosmology: observations — galaxies: clusters: general galaxies: halos —

## 1. INTRODUCTION

Cosmological simulations can be used to predict many different statistics of the mass distribution in the Universe. The most commonly employed statistic is the two-point correlation function, or its Fourier counterpart the power spectrum. Three-point statistics are much harder to predict and measure, and higher orders are rarely discussed. A more popular statistic is the number of peaks in the mass distribution, as given by the number of clusters of galaxies. The dark matter power spectrum and the number of clusters of galaxies are often cited as among the best ways to constrain the properties of dark energy (e.g. Albrecht et al. 2006).

Uncertainties on cosmological parameters are decreased when two measurements have different parameter degeneracies and are often referred to as ‘complementary’. In this paper we consider a statistic which may offer complementary constraints on cosmology: the *shapes* of peaks in the mass distribution, as probed by the ellipticity of galaxy cluster dark matter halos. In addition this may place important constraints on modifications to the law of gravity since we may compare the results from both dark and light matter, as also tested by studying the dark and light matter distributions in the bullet cluster (Clowe et al. 2006).

Predictions of cluster ellipticities come mostly from numerical simulations (West et al. 1989; de Theije et al. 1995; Jing & Suto 2002; Floor et al. 2003; Ho & White 2004; Flores et al. 2005; Rahman et al. 2006). The ellipticity is expected to depend on cosmological parameters (Evrard et al. 1993; Splinter et al. 1997; Buote & Xu 1997; Suwa et al. 2003; Rahman et al. 2004) and to evolve with redshift (Kasun & Evrard 2005; Allgood et al. 2006), an evolution which itself might depend on cosmology (Hopkins et al. 2005; Ho et al. 2006). The distribution of sub-halos within a cluster halo is

found to be an indicator of the overall halo ellipticity (Bode et al. 2007) but is slightly less elliptical.

The ellipticity of the brightest cluster galaxy and the ellipticity of the distribution of cluster member galaxies is much easier to observe than any other cluster ellipticity measure. This has been studied by a number of authors (West & Bothun 1990; Plionis et al. 1991; Rhee et al. 1991; Strazzullo et al. 2005). Most recently, Wang et al. (2007) studied groups of galaxies in SDSS and found an alignment between the brightest cluster galaxy (BCG) and the distribution of galaxies which was strongest in the most massive groups and between red BCGs and red group member galaxies.

In this paper we focus on measuring the dark matter ellipticity directly using gravitational lensing. We also compare this ellipticity to the ellipticity of the cluster member galaxy distribution, to see how reliable a tracer of ellipticity the light is, and therefore whether it can be used by itself for cosmological studies.

Gravitational lensing has been used very successfully to measure the mass and profile of clusters of galaxies by many authors. The work most relevant to our study is that of Sheldon et al. (2001); Sheldon et al. (2007b) and Sheldon et al. (2007a) who stack the lensing signal from many clusters of galaxies to find an average signal. Natarajan & Refregier (2000) proposed that when stacking the shear signal from many halos the stack could be made while retaining information about the major axis of the halo, as observed from the distribution of light. The stacked shear map should then provide a constraint on the ellipticity of the dark matter halo, if indeed the mass and light were aligned. They considered lensing by galaxies but we apply the same technique to clusters of galaxies here.

The ellipticity of the dark matter distribution has been studied observationally for galaxy sized halos using gravitational lensing using data from the Red-Sequence Cluster Survey (Hoekstra et al. 2004), the Sloan Digital Sky Survey (Mandelbaum et al. 2006) and the Canada-France-Hawaii Telescope Legacy Survey (Parker et al.

<sup>1</sup> Institute of Theoretical Astrophysics, University of Oslo, Box 1029, 0315 Oslo, Norway.

<sup>2</sup> Department of Physics and Astronomy, University College London, Gower Street, London, WC1E 6BT, UK.

2007). This has proved to be extremely difficult and we present here, for the first time, results from stacking galaxy cluster halos. Cypriano et al. (2004) has previously made measurements of the cluster dark matter ellipticity using gravitational lensing measurements from individual clusters. They found a good agreement between the dark matter halo orientation and the orientation of the brightest cluster galaxy.

When calculating angular diameter distances and the mean density of the Universe we assume a flat cosmology with  $\Omega_m = 0.3$ . The NFW halo profile has a very weak dependence on the fluctuation amplitude. We assume  $\sigma_8 = 0.8$  for this calculation.

The structure of this paper is as follows. In Sec. 2 we describe our data set and operations we have performed on the data such as rotating and stacking and removal of neighboring clusters. In Sec. 3 we use two theoretical models - a Singular Isothermal Ellipsoid (SIE) and a Navarro-Frenk-White (NFW, see Navarro et al. 1997) model - of the mass and light distribution, and look at correction factors from the redshift distribution and cluster decontamination. Our results, and some interpretations of these, are presented in Sec. 4. Conclusions are summarized and discussed in Sec. 5.

## 2. DATA

In this section we describe the catalogues used and the operations we carried out before comparing with models, including cluster selection and stacking and rotating.

### 2.1. Catalogues

We use the cluster catalogue of Koester et al. (2007a), which is at the present time the largest existing galaxy cluster catalogue, consisting of 13,823 galaxy clusters from the Sloan Digital Sky Survey (York et al. 2000). The cluster galaxies are red-sequence members (occupying the so-called E/S0 ridgeline in colour-magnitude space), brighter than  $0.4L_*$  in the  $i$  band and between redshifts  $0.1 < z < 0.3$ . They also lie within a circular aperture of radius  $R_{200}$ , which is the estimated radius within which the density of galaxies with  $24 < M_r < 16$  is 200 times the mean density of such galaxies. The number of cluster members inside this aperture is  $10 \leq N_{\text{gals}}^{r200} \leq 188$ ; the lower limit is a requirement for inclusion into the catalogue. We refer to Koester et al. (2007a) for details of the catalogue and to Koester et al. (2007b) for a description of the cluster selection algorithm.

In order to define an isolated sample, we removed clusters found to be too close to each other, as seen on the sky. Details on this close neighbour removal can be found in Sec. 2.2. Clusters that are too close to the survey edge are also removed, with the requirement that the minimum distance from the cluster center to the survey edge is  $7h^{-1}$  Mpc. We are left with a total of 4281 clusters to analyse for our purposes. We have also organised the clusters into 4 redshift bins between  $z = 0.10$  and  $z = 0.30$ , each of width 0.05 in  $z$ . Since these cluster redshifts are photometric, with uncertainties of  $\sim 0.01$  (Koester et al 2007a), the spectroscopic bin width will be very slightly larger than the photometric bin width. We do not take into account this small broadening in our analysis because we expect it to have negligible effect on the ellipticity results.

The shear galaxy catalogue is the same as used in Sheldon et al. (2004), except that the area covered is larger,  $\sim 6325 \text{ deg}^2$ . There is approximately one galaxy per square arcminute in this catalogue. Galaxies in the shear catalogue have extinction-corrected  $r$ -band Petrosian magnitudes less than 22. Stars have been removed from the catalogue by the Bayesian method discussed in Scranton et al. (2002). Unresolved galaxies and objects with photo- $z$  errors greater than 0.4 have also been removed. To correct the shapes of galaxies for effects of PSF dilution and anisotropy, the techniques of Bernstein & Jarvis (2002) were used, with modifications specified in Hirata & Seljak (2003). We refer to Sheldon et al. (2004) for full details of the compilation of the shear catalogue.

We do not want to include in the shear catalogue galaxies which are already in the cluster member catalogue. Therefore we remove from the shear catalogue all galaxies which are close, as seen on the sky, to a cluster member. We cut on a physical (as opposed to angular) distance of  $0.012 h^{-1}$  Mpc, as calculated at the redshift of the cluster. This distance corresponds to 5 arcseconds at redshift  $z = 0.2$ . In principle this cut may also remove some real background galaxies, however the shear measurements of these galaxies will in any case likely be adversely affected by the light contamination by the cluster members. Note that we do not eliminate *all* cluster members from the shear catalogue with this cut, only those clusters that fit the selection criteria set by the maxBCG selection method (red galaxies, brighter than  $0.4 L^*$ ; Koester et al. 2007a).

### 2.2. Postage stamp size and close neighbor removal

In order to avoid contamination of the shear signal from neighboring structures, we only include in our analysis galaxies which are sufficiently close to a cluster, as seen on the sky. We decide this distance by considering the predicted contribution of neighboring clusters to the shear signal, and then use this to decide the required separation of neighboring clusters.

We include in our shear catalogue galaxies in a square postage stamp of  $10 \times 10 h^{-1}$  Mpc centered on each cluster. This choice was made using Fig. 8 of Johnston et al. (2007), which shows model fits for the lensing signal split up into contributions from several components. We want the lensing signal in our postage stamp to be dominated by the central cluster, not by the contribution from neighboring mass concentrations such as nearby clusters and filaments. Our interest therefore lies in comparing their NFW profile (green line) to the contribution from neighboring halos (blue line). The results in their Fig. 8 are shown for 12 richness ( $N_{\text{gals}}^{r200}$ ) bins. The mean of the  $N_{\text{gals}}^{r200}$  values of our cluster sample is  $\sim 24$ , directing us to the panel  $N_{\text{gals}}^{r200}[18 - 25]$ . We match our postage stamp limit at the radius where the NFW contribution is roughly equal to that of the contribution from neighboring clusters. Note that we are also removing close neighbors (see below), so the contribution from neighboring halos would actually be even lower for our case, so our cut may be conservative.

Clusters that are *too* close to each other in projected

separation represent a challenge for our analysis. The mass distribution of a cluster will affect the shear field of its neighbor. This could have a significant effect on the measured ellipticity. While it is possible to isolate clusters in three dimensions within a simulation, we are plagued by overlaps on the sky since gravitational lensing measures the projected mass. We therefore endeavor to remove this complication by selecting relatively isolated clusters for this analysis. For proper comparison with theory, a similar sample should be made from simulations. However, in this paper we are primarily concerned with the first significant detection of ellipticity in a large sample.

We do not want the shear from a neighbor to appear within our postage stamp, but this is unavoidable to some extent, because the shear at one point is affected by mass far away (shear is non-local). The effect on the measured ellipticity of having neighbors is twofold: (i) It can make the distribution more circular, if the neighbor position is uncorrelated with cluster major axis. This will occur due to chance alignments close to the line of sight, particularly from clusters in different redshift bins; (ii) It can make the distribution more elliptical, if the neighbor position is correlated with major axis direction. Pairs of clusters which are physically close will probably be aligned along the major axis of the cluster (e.g. Plionis et al. 1991).

We therefore remove clusters that are closer than  $5h^{-1}$  Mpc (corresponding to half the width of the postage stamp) to neighboring clusters. When a cluster has one or more neighbors with an angular separation corresponding to less than  $5h^{-1}$  Mpc, calculated at the middle of the redshift bin of the cluster (see later), we discard it if any of the neighbors have a higher  $N_{\text{gals}}^{r200}$ . The neighbor removal was done consecutively from low to high redshift. This process reduced the number of available clusters to 4281. In a later section, we analyze the use of different minimum close neighbor distances.

Although we remove a cluster's less rich neighbors from our sample, the shear pattern of the remaining cluster will already have been affected by its neighbor(s). However, by retaining the richest of the neighboring clusters we hope that the shear field is dominated by this cluster.

### 2.3. Stacking and rotating

On average, we have only around 1 shear galaxy per square arcminute and the uncertainty on the shear for a single galaxy is an order of magnitude larger than the shear we are trying to measure. Therefore we need to use the shear signal from many clusters in order to obtain a significant signal. We therefore stack the clusters on top of each other to improve the signal-to-noise ratio. In other words, we use information from the postage stamp field of shear galaxies for all clusters simultaneously.

The stacking could be carried out in either physical or angular space. For our method the two approaches are exactly equivalent if the redshift bins are small enough. We stack in angular space and use redshift bins of redshift width 0.05. This causes a radial blurring because two clusters of the same physical size will be stacked on top of each other in angular space to have different angular sizes. The blurring of the shear and light maps will be of at worst plus and minus 20 per cent (for the low-

est redshift bin). Since superposing ellipses of different scalings retains the original ellipticity, this results in a slightly smoother cluster profile but will not affect our ellipticity results. We find that our results are fairly similar even when comparing two very different profiles, see Sec. 3.

Straightforward stacking of elliptical clusters with random orientations would erase any ellipticity and produce a circular average cluster. Before stacking, we therefore rotate each cluster to lie along an  $x$ -axis, which is the major axis as defined by the ellipticity of the cluster members, see Fig. 1. This rotate-and-stack method is described by Natarajan & Refregier (2000) for use in galaxy-galaxy lensing, and we have, for the first time, applied this technique for use on cluster lensing.

We calculate the direction of a cluster major axis from the positions of the cluster members, as defined in the cluster catalogue. We do not take into account the luminosity of each cluster member. The cluster center ( $x_c, y_c$ ) was taken to be the position of the brightest cluster galaxy (BCG) as defined by the maxBCG algorithm (Koester et al. 2007b). However, the position of the BCG is not necessarily coincident with the cluster's actual centre of mass. For comparison, we therefore calculate the center of each cluster as given by the mean position of the cluster members. The mean physical offset (for redshift bin  $0.20 < z < 0.25$ ) between the two center definitions is  $\sim 0.15h^{-1}$  Mpc, and the standard deviation  $0.09h^{-1}$  Mpc. Compared to our mask radius of  $0.5h^{-1}$  Mpc, therefore, the shift in centre position is relatively small. Any effect this mis-centering does have will increase the ellipticity of the members, which we do not focus on here, and cause the misalignment angle to tend towards the direction from the BCG to the center of the cluster member distribution. This would in itself be an alternative and potentially useful way to stack the clusters to obtain the results presented here. Therefore we do not consider this effect further.

To find the ellipticity angle of rotation of the cluster, we use the quadrupole moments of the cluster members. The quadrupole moments are given by:

$$Q_{xx} = \langle (x_i - x_c)^2 \rangle_i \quad (1)$$

$$Q_{xy} = \langle (x_i - x_c)(y_i - y_c) \rangle_i \quad (2)$$

$$Q_{yy} = \langle (y_i - y_c)^2 \rangle_i \quad (3)$$

where the summation  $i$  is over the cluster members. We convert this into the ellipticity components  $e_1$  and  $e_2$  of the cluster through the relations:

$$e_1 = \frac{Q_{xx} - Q_{yy}}{Q_{xx} + Q_{yy} + 2\sqrt{Q_{xx}Q_{yy} - Q_{xy}^2}} \quad (4)$$

$$e_2 = \frac{2Q_{xy}}{Q_{xx} + Q_{yy} + 2\sqrt{Q_{xx}Q_{yy} - Q_{xy}^2}}. \quad (5)$$

The angle of the cluster, anticlockwise from positive  $x$  axis, is then:

$$\theta^{\text{rot}} = \frac{1}{2} \tan\left(\frac{e_2}{e_1}\right). \quad (6)$$

We rotate the positions of the cluster member galaxies and the positions of the shear galaxies using the following

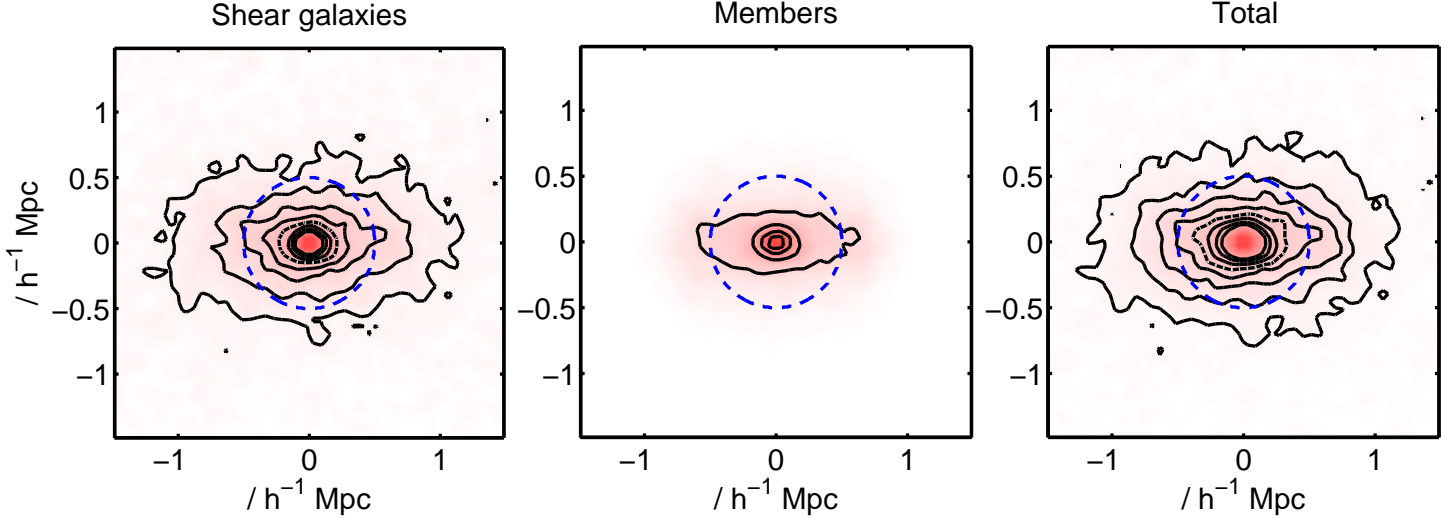


FIG. 1.— Total number of galaxies per unit area for redshift bin 3 ( $0.20 < z < 0.25$ ) for illustration. From left to right: shear galaxies, cluster members and total galaxies (shear galaxies plus cluster members). The left and right panels include galaxies which are uncorrelated with the cluster. We draw our contours relative to the constant background level (which is the same number in both left and right panels, since the cluster member catalogue does not contribute). For the left and right panels, contours are equally spaced from 1.2 to 2.6 times the background level, in steps of 0.2. The dashed contour shows 2 times the background level. For the central panel the contours are 0.2, 0.4, 0.6, 0.8 times the same background level. The dashed circle shows location of mask, see text. For comparison, a  $3 \times 10^{14} h^{-1} M_{\odot}$  cluster at a redshift of 0.2 has  $R_{200} \sim 1.4 h^{-1}$  Mpc, where  $R_{200}$  is the radius within which the mean density of the cluster is 200 times the mean matter density at the cluster redshift. We have zoomed in to show the central part of the postage stamp for clarity.

transformation

$$x^{\text{rot}} = d \cos(\theta - \theta^{\text{rot}}) \quad (7)$$

$$y^{\text{rot}} = d \sin(\theta - \theta^{\text{rot}}) \quad (8)$$

where  $(d, \theta)$  are the polar coordinates of the galaxy to be rotated, relative to the cluster center. For clusters with ellipticities close to zero,  $\theta^{\text{rot}}$  in Eq. 6 has little meaning. From the cluster members alone, 18% of our clusters have an ellipticity ( $e = \sqrt{e_1^2 + e_2^2}$ , using Eqs. 4 and 5) of less than 0.1 and only 5% have ellipticities less than 0.05. Therefore the angle is reasonably well defined. 2% of the clusters have an ellipticity greater than 0.5. The cluster selection criteria by Koester et al. (2007a) and/or our isolation criteria have therefore done a reasonable job of identifying isolated clusters. In addition the clusters seem relatively undisturbed, i.e. have low ellipticity. This also illustrates that it would not be particularly useful to bin the clusters according to the cluster member ellipticity because the range is relatively small (and our final signal to noise is quite low).

Fig. 1 shows the number of galaxies per unit area, for  $z$  bin 3, after stacking and rotating. The left panel shows galaxies from the shear galaxy catalogue, with cluster member catalogue galaxies removed, the middle panel shows cluster galaxies from the cluster member catalogue and the right panel shows the sum of shear galaxies and cluster members.

The left hand panel clearly contains a significant number of cluster members, despite the fact that the galaxies from the cluster member catalogue are not included. As described in Koester et al. (2007b), cluster members for this catalogue were identified using the maxBCG algorithm. This algorithm employs the red sequence method, based on the observational fact that cluster galaxies occupy a narrow region (a so-called *ridgeline*) in a colour-magnitude diagram. This method is designed to conservatively select red galaxies at the central area of a cluster.

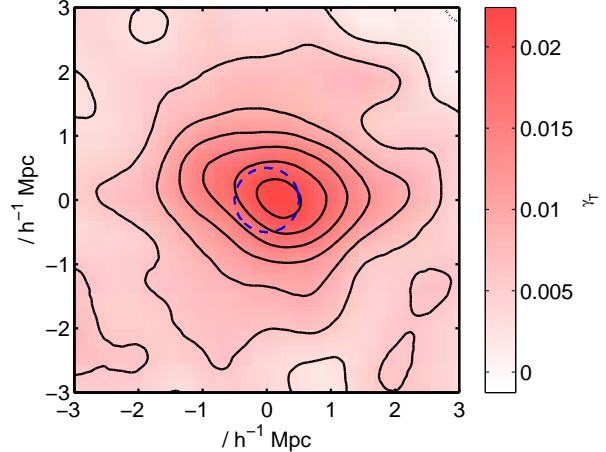


FIG. 2.— Tangential shear,  $\hat{\gamma}_T$ , as measured from all galaxies in the background galaxy catalogue from a zoomed-in view of the postage stamp. To reduce the noise we have smoothed with a Gaussian with standard deviation  $1 h^{-1}$  Mpc. The location of the mask is shown by the dashed circle.

As an illustration we investigate the central region of the stacked cluster in the third redshift bin ( $0.2 < z < 0.25$ ). In the central square arcminute the number of galaxies in the member catalogue is  $\sim 40\%$  of the number of galaxies in the (members removed) shear catalogue, after subtracting the constant background level i.e. most of the cluster members are not in the cluster member catalogue.

The existence of these extra members allows a very convenient check on our stacking and rotating: the rotation angles were calculated from the cluster member catalogue alone, whereas the left hand panel does not include the galaxies used to decide the rotation angle. Therefore the fact that we see ellipticity in this panel means that the angle calculated from the members catalogue is correlated with the angle of the extra cluster

members. If, for example, we had calculated rotation angles from a very small number of galaxies from the cluster member catalogue, there would be a large degree of randomness due to shot noise, and the alignment of measured and true ellipticity would be random to a large extent, resulting in a circular pattern in the left panel of Fig. 1.

The object of this paper is to calculate the ellipticity of the dark matter, as measured from gravitational lensing, and compare it with that of the light-emitting galaxies. Any misalignment in the stacking and rotating will tend to make the dark matter appear less elliptical. However this misalignment will have the same effect on the ellipticity of the light, as measured from the extra cluster members (left hand panel) alone. Therefore we can compare like with like, and assess the *relative* ellipticity of the dark and light matter, despite any misalignment.

We have chosen the contour levels so that a fair comparison can be made between the left and central panels: the outermost contour corresponds to the same cluster member density in each. Therefore we see that at large radii most of the cluster members are not included in the cluster member catalogue. For all the axis ratio measurements reported in this paper we exclude the central regions (see Sec. 3.3), this is shown by the dashed circle in Fig 1. Outside this excluded region we see that the contours change only a little from the left to the right panel. This is convenient because it means that it is not too important whether we compare the dark matter ellipticity with the light ellipticity derived from either the left or the right hand panel.

We calculate the tangential,  $\hat{\gamma}_T$ , and cross,  $\hat{\gamma}_X$ , components of the shear  $\hat{\gamma}$  for each shear galaxy

$$\hat{\gamma}_T = \hat{\gamma} \cos(2\alpha) \quad (9)$$

$$\hat{\gamma}_X = \hat{\gamma} \sin(2\alpha) \quad (10)$$

where  $\alpha$  is the angle between the shear galaxy major axis and a tangent through the center of the shear galaxy, with respect to the cluster center. We calculate the shear estimate for each galaxy from the polarizations ( $\epsilon$ ) in the shear galaxy catalogue

$$\hat{\gamma} = \frac{1}{2S_{\text{Sh}}} \epsilon \quad (11)$$

where the factor  $S_{\text{Sh}} \sim 0.88$  is the average responsivity of the source galaxies to a shear, see Sheldon et al. (2001) and references therein, and  $\epsilon = (a^2 - b^2)/(a^2 + b^2)$ , where  $a$  is the semi-major and  $b$  the semi-minor axis of the shear galaxy. We have redone our main NFW dark matter ellipticity result using a value  $S_{\text{Sh}}$  which is twenty per cent higher, and find only a negligible change. Note that the tangential and cross shears are invariant with respect to rotation of the cluster coordinates. We bin the shear galaxy catalogue into square pixels of size  $0.4 \times 0.4$  arcmin on the sky, but our main results are insensitive to this exact value. We average the shear estimates in each pixel.

Fig. 2 shows the smoothed tangential shear. As expected, the tangential shear is largest in the cluster center. To interpret this figure further it is helpful to consider the tangential and cross shears pattern predicted from popular cluster models, discussed further in Section 3. Cluster ellipticity causes little, if any, cross shear, depending on the cluster profile. For an elliptical SIE the

cross shear is exactly zero. For an elliptical NFW with a major to minor axis ratio of 0.5 (our best fit result), a mass of  $1 \times 10^{14} h^{-1} M_\odot$  and cluster redshift 0.15, the maximum cross shear occurs when approaching the center of the lens. Just outside our mask radius of  $0.5h^{-1}$  Mpc, the maximum cross shear is 0.0012 for a source redshift of 0.3. This value is 10 per cent of the maximum tangential shear outside the mask, and is therefore small compared to our uncertainties. The main effect of cluster ellipticity is to produce an ellipticity in the tangential shear map. Therefore the tentative visual indication of some horizontal elongation in this figure is our first hint of dark matter ellipticity.

To compare the data with models we must incorporate the errors on the shear estimates. The errors on the shear measurements are given by

$$\sigma_{\gamma_T}^2 = \sigma_i^2 + \sigma_{\text{SN}}^2 \quad (12)$$

where  $\sigma_i$  is the uncertainty in the shape measurement due to the finite number of photons falling in each detector element, plus detector noise, and  $\sigma_{\text{SN}}$  is the ‘shape noise’ due to intrinsic variance in the unlensed galaxy shapes (assumed the same for all galaxies).

We calculate the shape measurement uncertainty  $\sigma_i$  from the uncertainties in the two components of the ellipticity  $e_1$  and  $e_2$  using

$$\sigma_i = \frac{1}{2S_{\text{Sh}}} \frac{\sigma_{e1} + \sigma_{e2}}{2}. \quad (13)$$

The first factor converts from  $e$  to  $\gamma$  and the second part assumes that the uncertainty on the two ellipticity components is essentially equal and uncorrelated, which is approximately true for some shear estimators (e.g. Fig. 2 of Bridle et al. 2002). If these assumptions are true then it follows that the ellipticity uncertainty on a component is independent of rotation.

We estimate the shape noise  $\sigma_{\text{SN}}$  by calculating the rms dispersion in  $\hat{\gamma}_T$  values as a function of  $\sigma_i$ . We compare this to  $\sigma_{\gamma_T}$  for various  $\sigma_{\text{SN}}$  values and find  $\sigma_{\text{SN}} = 0.24$  to be the best fit.

To find the error on the shear for each pixel we take the mean of the errors  $\sigma_{\gamma_T}$  and divide by the square root of the number of galaxies in the pixel. Galaxies will have a range of sizes and therefore of measurement errors. When we calculate the average shear in each pixel we do not weight the galaxies according to their ellipticity errors. This is because this would tend to upweight the better measured galaxies. As better measured galaxies may preferentially tend to be cluster members that have leaked into the shear galaxy catalogue, this might preferentially weight up cluster members. This would have to be taken into account when removing the bias on the shear due to cluster member contamination (see Sec. 3.3), which would be difficult. We therefore use all the galaxies in the shear galaxy catalogue without weighting. Due to the cuts already made in creating the shear galaxy catalogue, the difference in weight between the noisiest and least noisy galaxies is only 30% therefore the weighting would not make a large difference to our analysis.

### 3. MODELLING

#### 3.1. Mass and light distributions

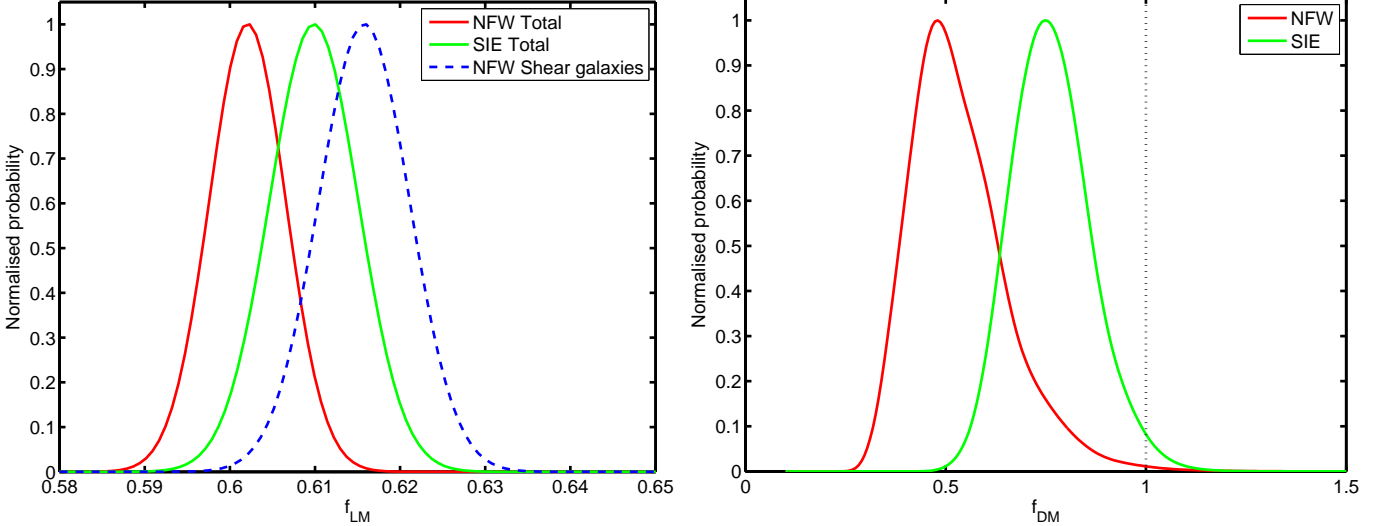


FIG. 3.— Left panel: Relative probability distribution of the axis ratio  $f_{LM} = b/a$  for the galaxy number density map from the shear catalogue plus member catalogue, thus including all cluster members. This includes clusters at all redshifts for an NFW model (dark, red line) and a SIE model (light, green line). The dashed line shows the result from shear catalogue galaxies only (for an NFW model). Right panel: Relative probability distribution for the dark matter axis ratio  $f_{DM}$ . The dark, red line shows result from the NFW model, and the light, green line shows result from the SIE model. The dotted vertical line shows  $f_{DM} = 1$  corresponding to a circular distribution.

The shear of galaxies depends on the mass and structure of the cluster acting as a lens. To model the cluster mass distribution, we use two alternative theoretical models: a Singular Isothermal Ellipsoid (SIE) and a Navarro-Frenk-White (NFW) model. The NFW model is preferred from simulations, but we also include results from the simpler SIE model to show an extreme and simple example of the dependence of our results on the cluster profile.

The SIE model corresponds physically to a distribution of self-gravitating particles with a Maxwellian velocity distribution with one-dimensional velocity dispersion  $\sigma_v$ . The convergence (normalized mass density)  $\kappa = \Sigma/\Sigma_{\text{crit}}$  of an SIE is given by

$$\kappa = 2\pi \frac{\sigma_v^2}{c^2} \frac{D_{\text{ds}}}{D_s} r^{-1} \quad (14)$$

where  $r$  is the generalized radius

$$r = (x^2 f + y^2 f^{-1})^{1/2} \quad (15)$$

and  $f = b/a$  is the axis ratio of the ellipse ( $b < a$ ),  $\sigma_v$  is the velocity dispersion and  $c$  is the speed of light.  $x$  and  $y$  are coordinates in the plane of the sky, at the cluster redshift. The distances  $D_{\text{ds}}$  and  $D_s$  are the angular diameter distances between the lens (deflector) and the source, and from the observer to the source, respectively. The SIE peaks sharply in the central parts, but we mask out the central regions (see Sec. 3.3). For the SIE model, we have the simple relation that the normalized surface density equals the tangential shear  $\gamma_T = \kappa$  (Kassiola & Kovner 1993; Kormann et al. 1994).

The NFW model is a more complicated but more realistic model based on numerical simulations. In order to implement the NFW, we need the projected mass of the cluster. To calculate the projected mass we use the equations given in Wright & Brainerd (2000) and Bartelmann (1996) using our generalized radius of Eq. 15 to make the cluster mass distribution elliptical. We use  $M_{200}$ , the mass enclosed within the radius at which the density

is 200 times the mean density of the Universe, for consistency with simulations. We derive the concentration parameter,  $c$ , where  $c \propto M^\beta$  according to Eq. 12 of Seljak (2000), where we interpret the virial mass  $M$  as  $M_{200}$ . We use  $\beta = -0.15$ , as appropriate for an NFW model. The shear for an elliptical mass distribution is calculated using the equations in Keeton (2001) which are derived from those in Schramm (1990). A shear map using these equations is illustrated in Fig. 1 of Bridle & Abdalla (2007).

We calculate probability as a function of our free parameters in each redshift bin, and marginalise over all but the axis ratio  $f$ . We then obtain a single result for  $f$  from combining all the redshift bins by multiplying the probabilities from different redshift bins together for each  $f$  value. This is the correct calculation if we believe that the other parameters have different values in each redshift bin, but that  $f$  is the same for all redshift bins.

### 3.1.1. Estimation of the light matter axis ratio ( $f_{LM}$ ) using galaxy positions

When stacking the clusters (Sec. 2.3), we calculated individual cluster ellipticities based on the cluster galaxies in the members catalogue. We do not use these results as our measure for the light matter ellipticity for the stacked cluster because they are relatively noisy due to the small number of members ( $\sim 10$  for the least rich clusters). Furthermore, we know that the members catalogue does not in fact contain all the cluster members, and has some selection criteria that may affect the ellipticity (requirement on proximity to cluster centre). We therefore use a  $\chi^2$  analysis to find the light matter ellipticity of the clusters. We model the light map as coming from (i) non-cluster galaxies which have a constant density across the postage stamp plus (ii) a contribution from the cluster galaxies which is assumed to have a galaxy density proportional to the mass profiles of Eq. 14

$$n^{\text{Pred}}(\mathbf{r}) = K\kappa(\mathbf{r}) + n_0 \quad (16)$$

where  $n_0$  is the background level of galaxies per pixel and  $K$  is a constant. Note that we do not assume that the light is some constant multiple of the mass, only that the light map is proportional to an SIE or NFW profile (which may have different parameters than the dark matter distribution). We do not tie the dark and light map parameters together because we wish to investigate whether the dark and light distributions both have the same ellipticity. For practical purposes we fix the mass at  $M_{200} = 10^{14} h^{-1} M_\odot$  in this calculation, which corresponds approximately to clusters of the mean richness we used (Johnston et al. 2007, Table 6). The value used affects the concentration parameter and therefore the mass profile of the cluster, which affects the weighting of the map. If we use a value a factor of ten higher our light ellipticity results change by less than one sigma and in any case our main results, on the dark matter ellipticity, are changed imperceptibly because the uncertainties on those are dominated by the much larger uncertainty on the dark matter quantities.

We calculate probabilities in the resulting three dimensional space ( $f_{\text{LM}}$ ,  $K$  and  $n_0$ ) by calculating a  $\chi^2$  between the predicted number (Eq. 16) and the observed number

$$\chi^2 = \sum_i \frac{(n_{\text{pred}}(\mathbf{r}_i) - n_{\text{obs}}(\mathbf{r}_i))^2}{\sigma_{n_i}^2} \quad (17)$$

and calculating probabilities from this;  $\text{Pr} = e^{\chi^2/2}$ .

Our assumption is that the errors are Poisson, therefore in the limit of large numbers the error on the number of galaxies, as used in the  $\chi^2$  calculation, is  $\sigma_{n_i} = \sqrt{n_{\text{pred}}(\mathbf{r}_i)}$ . We calculate our main results for each of the three stacked light maps shown in Fig. 1.

### 3.1.2. Estimation of the dark matter axis ratio ( $f_{\text{DM}}$ ) from the stacked shear map

To estimate the ellipticity of the dark matter distribution we calculate probability as a function of cluster axis ratio  $f_{\text{DM}}$  and cluster mass. We calculate the probability from the  $\chi^2$  between the observed and predicted shears, using the uncertainty on the shear values from Eq. 12. We marginalize over the cluster mass with a flat prior to obtain the probability as a function of the 2D axis ratio  $f_{\text{DM}}$ .

### 3.2. Redshift distributions

As discussed in Sec. 2, we divide our cluster sample up into four redshift bins. Due to the large photometric redshift uncertainties we decided not to use the redshift information in the shear galaxy catalogue. Therefore the ‘shear galaxies’ may be in front of, behind, or part of the cluster. The shear for each lens-source pair depends on the redshift of both the lens (cluster) and the source (shear galaxy). To calculate our theoretical model, we need a prediction for the distance ratio in Eq. 14 at each possible redshift. This must be averaged, weighted by the number of galaxies at each redshift. In other words, we need to calculate

$$\left\langle \frac{D_{\text{ds}}}{D_s} \right\rangle = \frac{\int_{z_L}^{\infty} (D_{\text{ds}}/D_s) n(z_s) dz_s}{\int_0^{\infty} n(z_s) dz_s}. \quad (18)$$

Note that the integration in the nominator starts at the lens redshift,  $z_L$ , so that galaxies between us and the lens

do not contribute to the shear signal, as they are not influenced by the presence of the cluster. We estimate  $n(z_s)$  from Fig. 3 and Eq. 8 in Sheldon et al. (2001), and as a result we use  $z_c = 0.22$ . However our results are quite insensitive to these numbers because we focus only on the ellipticity of the dark matter halo and not on its mass.

We obtain  $\langle D_{\text{ds}}/D_s \rangle = [0.51, 0.37, 0.26, 0.17]$  for the four redshift bins. The values are low for high redshift bins because a large fraction of the galaxies are between us and the cluster, and therefore do not contribute to the shearing effect. The calculation of  $D_{\text{ds}}/D_s$  is approximate because we assume all clusters to be located at the center of their redshift bin. However, this does not affect the ellipticity of the theory prediction. The distance ratio is incorporated into the predictions using Eq. 14.

### 3.3. Cluster decontamination

Because spectroscopic redshifts are not available for all shear catalogue galaxies, there will always be a degree of contamination by cluster members in the shear signal (as seen in Fig. 1(a)). Since we assume that the cluster members have no systematic alignment (but see Sec. 5 for an assessment of the implications of this assumption), members that have leaked into the shear galaxy catalogue will tend to dilute the shear signal. We correct for this dilution in our analysis. The corrected shear is given by

$$\gamma_{\text{cor}} = \frac{n(\mathbf{r})}{n_0} \hat{\gamma} \quad (19)$$

where  $n(\mathbf{r})$  is the total number of galaxies in the shear galaxy catalogue a two dimensional position  $\mathbf{r}$  from the center,  $n_0$  is the number of galaxies not in the cluster (see Eq. 16) and  $\hat{\gamma}$  is the observed, uncorrected shear. We use the best fit  $n_0$  value from the  $\chi^2$  fit to the light matter distribution. Inside the cluster, we have  $n(\mathbf{r}) > n_0$ , so the observed shear will be boosted by correcting for the contamination.

We mask the central regions from our analysis for several reasons. (i) In the very central regions, cluster members will obscure the shear galaxies. (ii) The cluster center may be incorrect and thus the central parts may appear erroneously circular after the stacking. (iii) There is actually an uncertainty associated with the correction factor that we have not taken into account. This error is due to Poisson fluctuations in the true number of non-cluster members per pixel, and will be more significant when the value of the correction factor is large, which occurs in the central region where the observed number of galaxies in the shear galaxy catalogue peaks sharply. For all these reasons, we mask out the central region using a circular mask with  $r_{\text{mask}} = 0.5 h^{-1} \text{ Mpc}$ . The radius of the mask was set where the correction factor increases above 1.5 (as calculated for  $0.20 < z \leq 0.25$ ), shown by the dashed circle in Fig. 1. This corresponds to 3.3 arcminutes at  $z = 0.225$ .

## 4. RESULTS

We now present our results on the stacked cluster ellipticity, focussing first on the NFW profile.

TABLE 1  
AXIS RATIO RESULTS FOR THE LIGHT MAPS

Population	$z$	SIE ( $f_{LM}$ )	NFW ( $f_{LM}$ )
Shear galaxies	$0.10 \leq z \leq 0.15$	$0.548 + 0.013 - 0.013$	$0.620 + 0.015 - 0.015$
	$0.10 \leq z \leq 0.15$	$0.555 + 0.014 - 0.014$	$0.614 + 0.012 - 0.013$
	$0.10 \leq z \leq 0.15$	$0.302 + 0.006 - 0.006$	$0.544 + 0.006 - 0.007$
Shear galaxies	$0.15 \leq z \leq 0.20$	$0.672 + 0.011 - 0.011$	$0.649 + 0.012 - 0.012$
	$0.15 \leq z \leq 0.20$	$0.657 + 0.012 - 0.011$	$0.631 + 0.010 - 0.010$
	$0.15 \leq z \leq 0.20$	$0.261 + 0.005 - 0.005$	$0.475 + 0.006 - 0.006$
Shear galaxies	$0.20 \leq z \leq 0.25$	$0.581 + 0.012 - 0.012$	$0.583 + 0.011 - 0.010$
	$0.20 \leq z \leq 0.25$	$0.578 + 0.011 - 0.010$	$0.575 + 0.009 - 0.009$
	$0.20 \leq z \leq 0.25$	$0.254 + 0.004 - 0.004$	$0.456 + 0.005 - 0.005$
Shear galaxies	$0.25 \leq z \leq 0.30$	$0.637 + 0.010 - 0.009$	$0.619 + 0.008 - 0.008$
	$0.25 \leq z \leq 0.30$	$0.624 + 0.008 - 0.008$	$0.602 + 0.007 - 0.007$
	$0.25 \leq z \leq 0.30$	$0.235 + 0.003 - 0.003$	$0.434 + 0.004 - 0.004$
Joint (total)	$0.10 \leq z \leq 0.30$	$0.610 + 0.005 - 0.005$	$0.602 + 0.004 - 0.005$

TABLE 2  
AXIS RATIO RESULTS FOR THE DARK MATTER DISTRIBUTION.

$z$	SIE ( $f_{DM}$ )	NFW ( $f_{DM}$ )
$0.10 \leq z \leq 0.15$	$0.754 + 0.230 - 0.186$	$0.614 + 0.400 - 0.176$
$0.15 \leq z \leq 0.20$	$0.522 + 0.159 - 0.115$	$0.269 + 0.158 - 0.054$
$0.20 \leq z \leq 0.25$	$0.958 + 0.251 - 0.199$	$0.599 + 0.379 - 0.208$
$0.25 \leq z \leq 0.30$	$0.853 + 0.306 - 0.215$	$0.614 + 0.444 - 0.266$
Joint analysis	$0.747 + 0.102 - 0.094$	$0.480 + 0.136 - 0.086$

#### 4.1. Results for the light matter axis ratio ( $f_{LM}$ )

The left panel of Fig. 3 shows the one-dimensional relative probability of the axis ratio  $f_{LM}$ , marginalised over  $K$  and  $n_0$  (see Eq. 16). The solid lines represent results from using the total cluster members, i.e. galaxies in both the shear galaxy catalogue and cluster member catalogue (corresponding to the right hand panel of Fig 1). The blue, dashed line shows results from using only the (members-removed) shear catalogue galaxies, corresponding to the left hand panel of Fig. 1, for the NFW model. This shows that the light matter distribution is clearly elliptical with an axis ratio of  $f_{LM} \sim 0.6$ . The errors on  $f_{LM}$  are calculated by finding the 68% iso-probability limits from the probability distribution  $P(f_{LM})$  after marginalizing over the other fit parameters. We find an error of  $\sim 0.005$ .

Table 1 shows three light matter ellipticity results for each redshift bin and for each theoretical model (SIE and NFW): (i) for the shear catalogue galaxies with cluster members removed, (ii) for the total cluster members (iii) for the cluster members and (members from the cluster catalogue plus the extra members included in the shear galaxy catalogue). The results from the NFW and SIE are qualitatively similar. The last line in Table 1 shows the joint results combining all bins, for the total cluster members.

There is a clear detection of ellipticity based on the number density of shear catalogue galaxies alone. We see that the distribution of galaxies in the members catalogue is more elliptical than that of the shear catalogue. This is not surprising because we stacked the galaxies according to the members catalogue. Even if the galaxies in the members catalogue had been sampled from a circular distribution then the finite number of galaxies would

provide a rotation direction so we would have in effect stacked the random noise to produce an ellipticity for the cluster members, while making the light map from the shear catalogue more circular.

This extra induced ellipticity could be simulated, but in fact there is no need because the axis ratio from the shear galaxy catalogue alone is very similar to that based on the total catalogue containing both the shear catalogue and the cluster member catalogue. Therefore we do not consider the results from only the cluster member catalogue any further.

The similarity of the ellipticities from the shear galaxy catalogue and the total catalogue is largely due to the fact that there are very few galaxies from the members catalogue outside our mask radius. The important conclusion for our paper is that any misalignment in the rotating and stacking will affect the light and dark matter ellipticity the same. The ellipticity observed in the light map makes us believe that the rotation angles are not completely random and therefore that we can hope to detect some ellipticity in the dark matter, if indeed the dark matter halo is elliptical.

#### 4.2. Results for the dark matter axis ratio ( $f_{DM}$ )

Ellipticity results for the dark matter analysis can be found in Table 2, for each individual redshift bin as well as for the joint result combining all redshift bins. For the NFW model, the joint result of  $f_{DM} = 0.48_{-0.09}^{+0.14}$  excludes a circular mass distribution ( $f_{DM} = 1$ ) by over  $3\sigma$  (if the probability distribution is Gaussian). The lowest axis ratio is in the second redshift bin ( $0.15 < z < 0.20$ ). We re-analyzed redshift bin 2 by dividing it into sub-bins, but found the result unchanged on removing the clusters with the lowest axis ratio. The joint result for the remaining redshift bins was then  $f_{DM} = 0.607_{-0.14}^{+0.21}$ . This is a weaker detection than our final result including the second redshift bin, but still a tentative detection of dark matter ellipticity.

The right panel of Fig. 3 shows the probability as a function of axis ratio for the dark matter distribution. The dark (red) line shows the result from using an NFW model, and the light (green) line shows the result from an SIE model. The vertical dotted line is showing  $f_{DM} = 1$ , which represents a circular mass distribution.

We can see from the figure that the probability is not totally Gaussian, with a tail to larger  $f_{DM}$  values. (Note

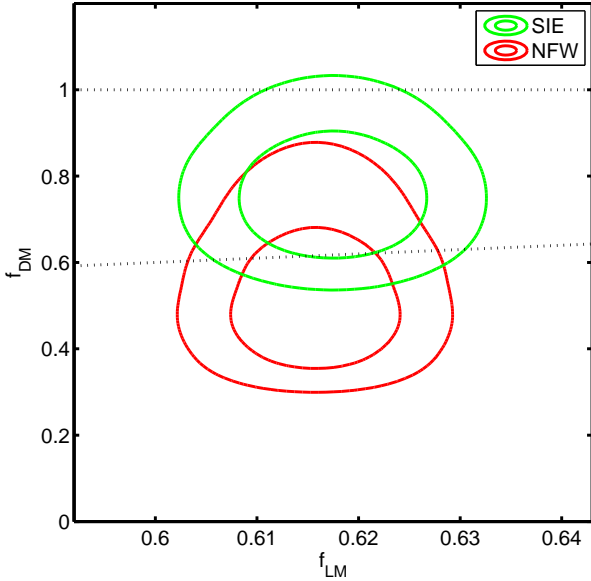


FIG. 4.— 68% and 95% contours of the two-dimensional probability distribution for the axis ratio of the dark matter ( $f_{\text{DM}}$ ) versus the axis ratio of the total galaxy number density distribution ( $f_{\text{LM}}$ , representing the light matter). Light (green) contours show the result from using an SIE profile as modelling the cluster, and dark (red) contours show result from using an NFW profile. The horizontal dotted line shows  $f_{\text{DM}} = 1$ , and the dotted line rising towards the right shows  $f_{\text{DM}} = f_{\text{LM}}$ .

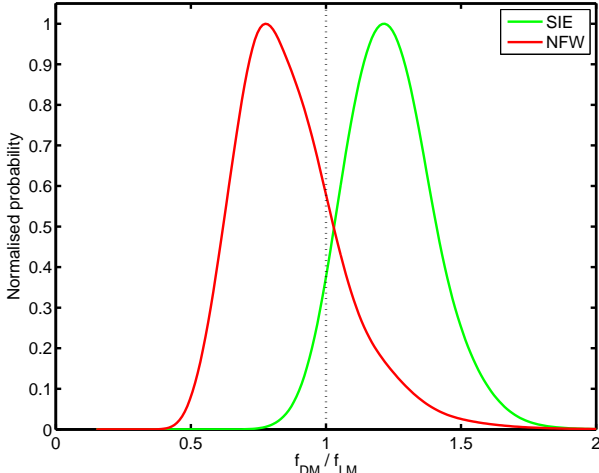


FIG. 5.— One-dimensional probability distributions as a function of the ratio  $f_{\text{DM}}/f_{\text{LM}}$ . Light (green) line is for the SIE result while dark (red) line is for the NFW result.

that an axis ratio greater than unity corresponds to an ellipse aligned along the  $y$  axis.) We find that 99.6 per cent of the probability is below  $f_{\text{DM}} = 1$ ; therefore we consider this to be a reasonable detection of dark matter ellipticity. Note that the best fit NFW result is quite a bit more elliptical than the SIE result, but the NFW result has a longer tail extending to higher  $f_{\text{DM}}$ -values than the SIE. For the SIE model 98.2 per cent of the probability is below  $f_{\text{DM}} = 1$ . The NFW is a more realistic profile, so we trust these results most.

Fig. 4 shows 68% and 95% contours of the two-dimensional probability distribution for the axis ratio of the dark matter ( $f_{\text{DM}}$ ) versus the axis ratio of the light

matter ( $f_{\text{LM}}$ ). The dotted lines also shown on the plot are  $f_{\text{DM}} = 1$  (horizontal dotted line) and  $f_{\text{DM}} = f_{\text{LM}}$  (dotted line rising towards the right). The two colors shown represent the different profiles used as cluster models: light (green) contours are for the SIE model, and dark (red) contours are for the NFW. We see that  $f_{\text{DM}} = 1$ , that is, a circular dark matter distribution, crosses just within the outermost (95%) contour for the SIE model and the NFW contours are both below the  $f_{\text{DM}} = 1$  line.

Fig. 5 shows the one-dimensional probability distribution as a function of the ratio of axis ratios of the dark and light matter:  $f_{\text{DM}}/f_{\text{LM}}$ . Again, the light (green) line is for the SIE model profile and the dark (red) line is for the NFW model. The vertical dotted line shows where we have  $f_{\text{DM}} = f_{\text{LM}}$ , that is; the axis ratio as deduced from the shear values equals the axis ratio as deduced from the distribution of the cluster galaxies. Both profiles are consistent with having the same ellipticity in the light and in the dark matter,  $f_{\text{DM}}/f_{\text{LM}} = 1$ . We find  $f_{\text{DM}}/f_{\text{LM}} = 0.91^{+0.19}_{-0.25}$  for the NFW model and  $f_{\text{DM}}/f_{\text{LM}} = 1.26^{+0.16}_{-0.17}$  for the SIE. The higher SIE result is driven by the larger  $f_{\text{DM}}$  for the SIE, which makes the dark matter distribution appear more round.

#### 4.3. Dependence on close neighbor distance

We made a decision to exclude all clusters with a more massive neighbor within an angular size corresponding to  $5h^{-1}$  Mpc at the cluster redshift. In this section we test how dependent our results are on this decision. Table 3 shows that our main result changes little as the cut is made 50 per cent smaller or larger. As expected, when a larger radius is used, fewer clusters survive in the catalogue, therefore the uncertainties become larger. Using a smaller radius does increase the ellipticity which is to be expected if the main effect is to include more physically associated clusters which are more likely to lie along the major axis of the cluster, perhaps due to formation along an intervening filament. We find similar results for the light ellipticity. Our main results are unchanged by changing the cluster isolation criterion.

#### 4.4. Misalignment simulations

In order to interpret our results we need to take into account possible misalignments during stacking. When we rotate clusters according to the distribution of the cluster members before stacking, we assume that the orientation of the light is correlated with the orientation of the mass. A result of  $f_{\text{DM}}$  consistent with 1 could indicate either a circular mass distribution or a random alignment between the light used for stacking and the dark matter. In the latter case, the circular result would be caused by the stacking of many clusters with different misalignments between the dark and the light matter.

In order to quantify this effect we simulate many clusters all with the same input axis ratio  $f_{\text{in}}$ . The misalignment angles between the light and the dark matter for the simulated clusters are random, with a standard deviation  $\sigma_{\theta}$ . For each value of  $f_{\text{in}}$  and  $\sigma_{\theta}$ , we rotate and stack the clusters in the same way as for the SDSS data. Therefore if  $\sigma_{\theta}$  is large, the input ellipticity will be smeared out a great deal and output axis ratio  $f_{\text{out}}$  will be close to unity. If  $\sigma_{\theta}$  is small the output ellipticity

TABLE 3  
EFFECT OF NEIGHBOR REMOVAL ON MEASURED ELLIPTICITY. RESULTS ARE SHOWN FOR THE NFW PROFILE ONLY.

Cut/ $h^{-1}$ Mpc	No. clusters	Light matter $f_{LM}$	Dark matter $f_{DM}$
2.5	6934	$0.587 + 0.004 - 0.004$	$0.459 + 0.155 - 0.077$
5	4281	$0.602 + 0.004 - 0.005$	$0.480 + 0.136 - 0.086$
7.5	2542	$0.625 + 0.006 - 0.006$	$0.614 + 0.205 - 0.139$

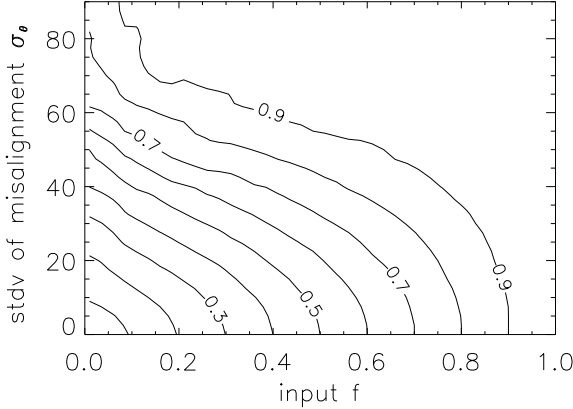


FIG. 6.— Contours show output axis ratios for simulated misalignments between the light and dark matter. Axes show input axis ratio  $f_{in}$  and standard deviation  $\sigma_\theta$  (in degrees) of the angle distribution of the simulated clusters.

will be more similar (or in the case of zero misalignment, equal) to  $f_{in}$ .

Fig. 6 shows the output dark matter axis ratio as a function of degree of misalignment  $\sigma_\theta$  and input axis ratio  $f_{in}$ . In order for the input ellipticity to be very elliptical ( $f \rightarrow 0$ ), the misalignment between the dark and light matter must be  $\sim 50^\circ$  for our dark matter  $f_{DM}$  of  $\sim 0.5$  (see Table 2). We conclude that the misalignment angle must be less than  $\sim 50^\circ$ . If there is any misalignment between the light and the dark matter, the dark matter will be even more elliptical than the results shown in the table and can be read off Fig. 6 for a given misalignment angle.

## 5. CONCLUSIONS AND DISCUSSION

We have used galaxy clusters from the catalogue of Koester et al. (2007a) and shear maps as used in Sheldon et al. (2004) to investigate the light and dark matter ellipticities of galaxy cluster halos. We rotate the selected clusters so that their major axes are aligned, and stack them according to the method which is described in Natarajan & Refregier (2000) for galaxy-galaxy lensing. This is the first time that this method has been applied to cluster lensing.

Through the pattern imprinted on the shear maps by intervening massive cluster halos, we have detected a dark matter ellipticity of these halos at a 99.6% level, with an axis ratio of  $f_{DM} = 0.48^{+0.14}_{-0.09}$  from a joint  $\chi^2$ -analysis for an NFW model, using 4281 clusters between  $0.10 < z \leq 0.30$ . We have corrected for dilution of the shear signal by cluster members left in the shear galaxy catalogues but have masked out the central areas where this correction factor grows too large.

The light matter distribution of the clusters, as traced by the number density of individual cluster members,

is also clearly elliptical, with a joint axis ratio  $f_{LM} = 0.60^{+0.04}_{-0.05}$  for the NFW model. Using the shear catalogue alone gives very similar results to using the shear catalogue concatenated with the cluster member catalogue, which means that we are essentially comparing like with like when comparing dark and light map ellipticities. This is because both the light matter (shear catalogue) and the dark matter have been stacked in the same way.

We find that the ellipticity of the dark matter distribution is consistent with the ellipticity of the galaxy number density distribution. Our result is limited by the uncertainty in the ellipticity of the dark matter distribution. The results for the NFW and SIE agree within the errors, but any differences could be attributed to a changing ellipticity with radius. We have not attempted to measure this effect since the uncertainties are too large.

Shear maps from neighboring clusters will influence each other, making the pattern more elliptical or less, depending on the redshift of the neighbors. In order to reduce this effect as much as possible, we use only the cluster with the highest number of members ( $N_{\text{gals}}^{>200}$ ) when two (or more) clusters are closer together than  $5h^{-1}$  Mpc, as seen on the sky. We find that increasing or decreasing the minimum distance to a close neighbor by 50 % does not significantly affect our main results.

We have also simulated the effect that a possible misalignment between the light and dark matter could have, and concluded that, according to our results, the light and dark matter must be misaligned by less than  $\sim 50^\circ$ .

Our measurement is very insensitive to overall calibration biases in shear measurements, since these are degenerate with cluster mass, rather than cluster ellipticity. It is unlikely that biases in shear measurement would vary with angle around the cluster: residual point spread function anisotropies would be oriented at random with respect to the cluster major axis and would cancel out on stacking; the cluster member light may leak into the postage stamps used to measure shears of background galaxies, but we remove the central region where the number of confirmed cluster members is significant.

Possibly the biggest potential systematic is intrinsic alignment of cluster members pointing at the cluster center (Ciotti & Dutta 1994; Kuhlen et al. 2007; Pereira et al. 2008; Knebe et al. 2008; Faltenbacher et al. 2008) which would be a problem for us because we have not made a significant attempt to remove cluster members from our analysis and our background catalogue is not particularly deep. A thorough assessment of this effect is beyond the scope of the current work. To first order this would make our observed shear maps less elliptical since the contamination by cluster members is greatest along the cluster major axis, and thus the strong gravitational shears expected along this axis will be partially cancelled

out by the cluster members which have the opposite ellipticity since they tend to point at the cluster center. However a full assessment of this effect would also have to take into account the variation in intrinsic alignment with respect to the cluster major axis, which appears to be more complicated (Kuhlen et al. 2007) and possibly weakens the degree of cancellation preferentially along the cluster major axis.

In Hopkins et al. (2005), the authors use a large-scale, high-resolution  $N$ -body simulation to predict cluster ellipticities and alignments in a  $\Lambda$ CDM universe. They find an ellipticity

$$\langle \epsilon \rangle = 1 - \langle f \rangle = 0.33 + 0.05z. \quad (20)$$

for the redshift range  $0 < z < 3$ . This redshift evolution is negligible for the redshift range considered here, and due to the large uncertainties we do not try to detect any trends with redshift. For a redshift in the middle of the redshift range of our cluster sample ( $z = 0.2$ ), this formula yields an axis ratio of  $f = 0.66$  which is in good agreement with our result of  $f_{\text{DM}} = 0.48^{+0.14}_{-0.09}$ .

Ho et al. (2006) have used numerical simulations of cluster formation with the aim of investigating the possibility of using cluster ellipticities as a cosmological probe. They find that the mean ellipticity of high mass clusters is approximated by

$$\bar{e}(z) = 0.245 \left[ 1 - 0.256 \frac{\sigma_8(z)}{0.9} + 0.00246 \frac{\Omega_m}{0.3} \right]. \quad (21)$$

Using  $\sigma_8(z) = 0.8$  and  $\Omega_m = 0.3$ , this gives an ellipticity of  $e \sim 0.2$ , or  $f \sim 0.8$ . This result is more circular than our main result. However, to make a proper comparison of our result with theory it would be necessary to make a theoretical prediction that takes into account our observation method, especially the overlaps in the shear field due to close neighbors and the impact of selecting the most isolated clusters.

Hoekstra et al. (2004) report on a first weak-lensing detection of the flattening of galaxy dark matter halos, using data from the Red-Sequence Cluster Survey. They find an average galaxy dark matter halo ellipticity of  $\langle \epsilon \rangle = 0.33^{+0.07}_{-0.09}$ . They also find a detection that dark matter halos are rounder than the light map. In a later work, Mandelbaum et al. (2006) did not find a definite detection of this effect in the larger SDSS dataset. However, Parker et al. (2007), measuring the ratio of tangential shear in regions close to the semi-minor versus that close to the semi-major axes of the lens, find some evidence of a halo ellipticity of  $\sim 0.3$  using early data from the Canada-France-Hawaii Telescope Legacy Survey (CFHTLS). Mandelbaum et al. (2006) commented that the stronger signal in clusters of galaxies means that there is more chance of making a detection of el-

lipticity in this higher mass data set. Therefore we have confirmed the detection of dark matter halo ellipticity, extending the measurement to cluster scales. We find no evidence for different ellipticities for the light and dark matter distribution on cluster scales.

Mandelbaum et al. (2006) focus on measuring the ratio of (dark matter) halo ellipticity to galaxy (light) ellipticity  $\epsilon_h/\epsilon_g$  where  $\epsilon = (a^2 - b^2)/(a^2 + b^2)$ . They find  $\epsilon_h/\epsilon_g = 0.60 \pm 0.38$  (68 per cent confidence) for elliptical galaxies, which is most comparable with our result of  $f_{\text{DM}}/f_{\text{LM}} = 0.91^{+0.19}_{-0.25}$  (68 per cent confidence) where  $f = b/a$ . Repeating our calculation using the different ellipticity parameters we find  $\epsilon_h/\epsilon_g = 1.37^{+0.35}_{-0.26}$ . It is expected that our value is greater than unity, since we find that the dark matter is more elliptical (lower axis ratio) than the light matter. However it is not significantly larger. The result of Mandelbaum et al. (2006) is the opposite side of unity, but the difference is not significant and we note that our result is for clusters and that of Mandelbaum et al. (2006) is for galaxies.

The anisotropy of the lensing signal around individual galaxies, if definitely detected, has been said to pose a serious problem for alternative theories of gravity (Hoekstra et al. 2004). For galaxy clusters it is more complicated, as the dominant source of baryons is the intracluster gas. Lensing by clusters has been found to pose a problem for Modified Newtonian Dynamics (MOND), as there seems to be a need to include a dark matter component (Sanders 2003; Takahashi & Chiba 2007).

Because the gas - the dominant baryonic component of clusters - is collisional, we can suppose that on cluster scales it will be less elliptical than the light. We may end up concluding that either (i) the gas distribution is elliptical (which we would not expect) or (ii) our result is inconsistent with MOND. However, further study and simulations of this is clearly needed.

We would like to thank Erin Sheldon and Benjamin Koester for providing us with galaxy catalogues and for very helpful comments and suggestions. We would also like to thank the anonymous referee for many helpful comments and suggestions. We would also like to thank Timothy McKay, Jochen Weller, Håkon Dahle, Andreas Jaunsen, Margrethe Wold, Shirley Ho, Eduardo Cypriano, Laurie Shaw, Richard Cook, David Sutton, Andrey Kravtsov, Øystein Elgarøy, Morad Amarzguioui, Terje Fredvik and Stein Vidar Hagfors Haugan for helpful discussions. AKDE acknowledges support from the Research Council of Norway, Project No. 162830. SLB acknowledges support from the Royal Society in the form of a University Research Fellowship.

## REFERENCES

Albrecht, A., Bernstein, G., Cahn, R., Freedman, W. L., Hewitt, J., Hu, W., Huth, J., Kamionkowski, M., Kolb, E. W., Knox, L., Mather, J. C., Staggs, S., & Suntzeff, N. B. 2006, ArXiv Astrophysics e-prints

Allgood, B., Flores, R. A., Primack, J. R., Kravtsov, A. V., Wechsler, R. H., Faltenbacher, A., & Bullock, J. S. 2006, MNRAS, 367, 1781

Bartelmann, M. 1996, A&A, 313, 697

Bernstein, G. M. & Jarvis, M. 2002, AJ, 123, 583

Bode, P., Ostriker, J. P., Weller, J., & Shaw, L. 2007, ApJ, 663, 139

Bridle, S. & Abdalla, F. B. 2007, ApJ, 655, L1

Bridle, S., Kneib, J.-P., Bardeau, S., & Gull, S. 2002, in The shapes of galaxies and their dark halos, Proceedings of the Yale Cosmology Workshop "The Shapes of Galaxies and Their Dark Matter Halos", New Haven, Connecticut, USA, 28-30 May 2001. Edited by Priyamvada Natarajan. Singapore: World Scientific, 2002, ISBN 9810248482, p.38, ed. P. Natarajan, 38 –

Buote, D. A. & Xu, G. 1997, MNRAS, 284, 439

Ciotti, L. & Dutta, S. N. 1994, MNRAS, 270, 390

Clowe, D., Bradač, M., Gonzalez, A. H., Markevitch, M., Randall, S. W., Jones, C., & Zaritsky, D. 2006, ApJ, 648, L109

Cypriano, E. S., Sodré, L. J., Kneib, J.-P., & Campusano, L. E. 2004, ApJ, 613, 95

de Theije, P. A. M., Katgert, P., & van Kampen, E. 1995, MNRAS, 273, 30

Evrard, A. E., Mohr, J. J., Fabricant, D. G., & Geller, M. J. 1993, ApJ, 419, L9+

Faltenbacher, A., Jing, Y. P., Li, C., Mao, S., Mo, H. J., Pasquali, A., & van den Bosch, F. C. 2008, ApJ, 675, 146

Floor, S. N., Melott, A. L., Miller, C. J., & Bryan, G. L. 2003, ApJ, 591, 741

Flores, R. A., Allgood, B., Kravtsov, A. V., Primack, J. R., Buote, D. A., & Bullock, J. S. 2005, ArXiv Astrophysics e-prints

Hirata, C. & Seljak, U. 2003, MNRAS, 343, 459

Ho, S., Bahcall, N., & Bode, P. 2006, Astrophys. J., 647, 8

Ho, S. & White, M. 2004, ApJ, 607, 40

Hoekstra, H., Yee, H. K. C., & Gladders, M. D. 2004, ApJ, 606, 67

Hopkins, P. F., Bahcall, N. A., & Bode, P. 2005, Astrophys. J., 618, 1

Jing, Y. P. & Suto, Y. 2002, ApJ, 574, 538

Johnston, D. E., Sheldon, E. S., Wechsler, R. H., Rozo, E., Koester, B. P., Frieman, J. A., McKay, T. A., Evrard, A. E., Becker, M. R., & Annis, J. 2007, ArXiv e-prints, 709

Kassiola, A. & Kovner, I. 1993, ApJ, 417, 450

Kasun, S. F. & Evrard, A. E. 2005, ApJ, 629, 781

Keeton, C. R. 2001, ArXiv Astrophysics e-prints

Knebe, A., Draganova, N., Power, C., Yepes, G., Hoffman, Y., Gottlöber, S., & Gibson, B. K. 2008, MNRAS, L40+

Koester, B. P., McKay, T. A., Annis, J., Wechsler, R. H., Evrard, A., Bleem, L., Becker, M., Johnston, D., Sheldon, E., Nichol, R., Miller, C., Scranton, R., Bahcall, N., Barentine, J., Brewington, H., Brinkmann, J., Harvanek, M., Kleinman, S., Krzesinski, J., Long, D., Nitta, A., Schneider, D. P., Snedden, S., Voges, W., & York, D. 2007a, ApJ, 660, 239

Koester, B. P., McKay, T. A., Annis, J., Wechsler, R. H., Evrard, A. E., Rozo, E., Bleem, L., Sheldon, E. S., & Johnston, D. 2007b, ApJ, 660, 221

Kormann, R., Schneider, P., & Bartelmann, M. 1994, A&A, 284, 285

Kuhlen, M., Diemand, J., & Madau, P. 2007, ApJ, 671, 1135

Mandelbaum, R., Hirata, C. M., Broderick, T., Seljak, U., & Brinkmann, J. 2006, MNRAS, 370, 1008

Natarajan, P. & Refregier, A. 2000, ApJ, 538, L113

Navarro, J. F., Frenk, C. S., & White, S. D. M. 1997, ApJ, 490, 493

Pereira, M. J., Bryan, G. L., & Gill, S. P. D. 2008, ApJ, 672, 825

Parker, L. C., Hoekstra, H., Hudson, M. J., van Waerbeke, L. & Mellier, Y. 2007, ApJ, 669, 21

Plionis, M., Barrow, J. D., & Frenk, C. S. 1991, MNRAS, 249, 662

Rahman, N., Krywult, J., Motl, P. M., Flin, P., & Shandarin, S. F. 2006, MNRAS, 367, 838

Rahman, N., Shandarin, S. F., Motl, P. M., & Melott, A. L. 2004, ArXiv Astrophysics e-prints

Rhee, G. F. R. N., van Haarlem, M. P., & Katgert, P. 1991, A&AS, 91, 513

Sanders, R. H. 2003, MNRAS, 342, 901

Schramm, T. 1990, A&A, 231, 19

Scranton, R. et al. 2000, ApJ, 579, 48

Seljak, U. 2000, MNRAS, 318, 203

Sheldon, E. S., Johnston, D. E., Frieman, J. A., Scranton, R., McKay, T. A., Connolly, A. J., Budavári, T., Zehavi, I., Bahcall, N. A., Brinkmann, J., & Fukugita, M. 2004, AJ, 127, 2544

Sheldon, E. S., Johnston, D. E., Masjedi, M., McKay, T. A., Blanton, M. R., Scranton, R., Wechsler, R. H., Koester, B. P., Hansen, S. M., Frieman, J. A., & Annis, J. 2007a, ArXiv e-prints, 709

Sheldon, E. S., Johnston, D. E., Scranton, R., Koester, B. P., McKay, T. A., Oyaizu, H., Cunha, C., Lima, M., Lin, H., Frieman, J. A., Wechsler, R. H., Annis, J., Mandelbaum, R., Bahcall, N. A., & Fukugita, M. 2007b, ArXiv e-prints, 709

Sheldon, E. S. et al. 2001, Astrophys. J., 554, 881

Splinter, R. J., Melott, A. L., Linn, A. M., Buck, C., & Tinker, J. 1997, ApJ, 479, 632

Strazzullo, V., Paolillo, M., Longo, G., Puddu, E., Djorgovski, S. G., De Carvalho, R. R., & Gal, R. R. 2005, MNRAS, 359, 191

Suwa, T., Habe, A., Yoshikawa, K., & Okamoto, T. 2003, ApJ, 588, 7

Takahashi, R. & Chiba, T. 2007, ApJ, 671, 45

Wang, Y., Yang, X., Mo, H. J., Li, C., van den Bosch, F. C., Fan, Z., & Chen, X. 2007, ArXiv e-prints, 710

West, M. J. & Bothun, G. D. 1990, ApJ, 350, 36

West, M. J., Dekel, A., & Oemler, A. J. 1989, ApJ, 336, 46

Wright, C. O. & Brainerd, T. G. 2000, ApJ, 534, 34

York, D. G. et al. 2000, AJ, 120, 1579